

G2P: Gaussian-to-Point Attribute Alignment for Boundary-Aware 3D Semantic Segmentation

Hojun Song^{*1} Chae-yeong Song^{*1} Jeong-hun Hong¹ Chaewon Moon¹ Dong-hwi Kim¹
 Gahyeon Kim¹ Soo Ye Kim² Yiyi Liao³ Jaehyup Lee¹ Sang-hyo Park^{†1}

¹Kyungpook National University ²Adobe Research ³Zhejiang University

<https://hojunking.github.io/webpages/G2P/>

Abstract

Semantic segmentation on point clouds is critical for 3D scene understanding. However, sparse and irregular point distributions provide limited appearance evidence, making geometry-only features insufficient to distinguish objects with similar shapes but distinct appearances (e.g., color, texture, material). We propose Gaussian-to-Point (G2P), which transfers appearance-aware attributes from 3D Gaussian Splatting to point clouds for more discriminative and appearance-consistent segmentation. Our G2P address the misalignment between optimized Gaussians and original point geometry by establishing point-wise correspondences. By leveraging Gaussian opacity attributes, we resolve the geometric ambiguity that limits existing models. Additionally, Gaussian scale attributes enable precise boundary localization in complex 3D scenes. Extensive experiments demonstrate that our approach achieves superior performance on standard benchmarks and shows significant improvements on geometrically challenging classes, all without any 2D or language supervision. Code will be released soon.

1. Introduction

Point cloud segmentation is a fundamental task that enables comprehensive 3D scene understanding across diverse real-world applications. Despite strong progress [7, 26, 48, 52], the intrinsic sparsity and irregular sampling of point clouds force models to over-rely on coarse geometry, leading to geometric bias that confuses objects with similar shapes but distinct appearances [20]. For instance, background-adjacent objects (e.g., doors, windows, refrigerators) that are coplanar with walls or floors often become indistinguishable from their surroundings in sparse point clouds (Fig. 1(a)). This geometric bias highlights the need to align

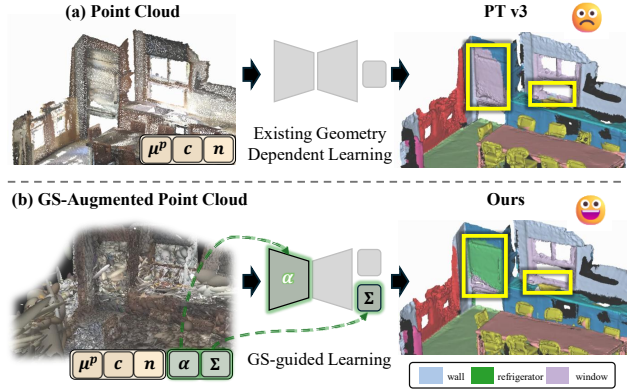


Figure 1. **G2P augments Gaussian attributes to points while preserving geometry.** (a) *Point Cloud*. Traditional point cloud representations lack sufficient appearance information to distinguish objects with similar geometry. As shown in the prediction, the existing model fails to segment coplanar windows cleanly and misclassifies the metallic refrigerator (yellow boxes), revealing geometric bias from insufficient appearance cues. (b) *GS-Augmented Point Cloud (ours)*. Through our novel Gaussian-to-Point feature augmentation, G2P enriches points with Gaussian attributes (Σ, α), which encode rich appearance and geometric information. This enables successful segmentation of both challenging cases, resolving the geometric bias problem.

appearance cues for accurate discrimination.

Recent advances have improved geometric understanding of point clouds, but existing approaches still face two fundamental limitations. **1) Boundary ambiguity.** Boundary-aware approaches [19, 47, 63] explicitly model edges, refining object boundaries. However, they remain limited to geometric reasoning and do not take advantage of the appearance information essential to address geometric bias [10, 15]. **2) Cross-modal misalignment.** 2D-3D fusion approaches [6, 16, 22, 40, 46] inject rich image features but suffer from structural mismatches [15]. The discrete nature of point clouds makes wire-like structures hard

^{*}Equal contribution. [†]Corresponding author.

to distinguish from flat surfaces [62], while projection introduces misalignment and occlusion-induced loss [20, 28]. These issues cause segmentation failures even for visually distinct regions, calling for a unified 3D representation that inherently encodes both geometry and appearance.

Among existing representations, 3D Gaussian Splatting (GS) [23] offers a promising direction that can address both geometric sparsity and appearance deficiency. Unlike point clouds with binary occupancy, Gaussian primitives possess continuous volumetric attributes that encode both geometric structure and appearance properties. Residing in the same 3D coordinate frame as points, these attributes can transfer with less spatial misalignment than 2D-3D fusion [28, 30, 60, 62]. However, optimization in GS often causes Gaussians to deviate from their initial positions [14, 23, 33, 43], creating a structural mismatch that prevents direct application of Gaussian attributes to point-level segmentation tasks.

To address this challenge, we introduce Gaussian-to-Point (**G2P**), which augments input points with Gaussian attributes while preserving their original geometry. As illustrated in Fig. 1(b), G2P creates appearance-aware point clouds by augmenting the original geometric information (μ^p, c, n) with GS-derived attributes (Σ, α) . This enables accurate segmentation of geometrically ambiguous objects that baseline methods tend to misclassify. Our G2P operates through three key components: (i) *Gaussian-to-Point Feature Augmentation* establishes precise correspondences via distance-based matching that accounts for anisotropic Gaussian ellipsoids; (ii) *GS Primitives-guided Learning* transfers view-consistent material cues to mitigate the point-level geometric bias; and (iii) *Scale-based Boundary Extraction* exploits anisotropic distributions to generate edge-aware pseudo-labels.

We conduct comprehensive experiments on multiple benchmark datasets. Our G2P consistently outperforms existing methods overall without any auxiliary supervision and achieves significant improvements on geometrically challenging classes. In summary, our main contributions are as follows:

- We introduce G2P, the first approach that directly leverages aligned 3D Gaussian Splatting attributes for point cloud semantic segmentation.
- We leverage appearance information in the native 3D space, bypassing cross-modal fusion limitations through Gaussian opacity-guided feature distillation.
- We enhance segmentation accuracy via scale-based boundary extraction that leverages anisotropic Gaussian distributions.

2. Related Works

2.1. 3D Point Cloud Segmentation

3D point cloud semantic segmentation has evolved from early per-point methods [29, 36, 51] to sophisticated architectures. PointNet++ [37] introduces hierarchical set abstraction for multi-scale learning, while MinkUNet [7] transforms point clouds into voxels and employs sparse convolutions to deliver robust and scalable segmentation. Recently, transformer-based architectures such as OctFormer [48] and Point Transformer v3 [52] have demonstrated state-of-the-art performance through efficient self-attention mechanisms.

Beyond supervised learning, self-supervised approaches like PointContrast [55] leverage contrastive learning, while Sonata [53] demonstrates effective pre-training on large-scale 3D datasets. Despite these advances, purely geometric approaches suffer from boundary ambiguity and geometric bias in sparse point clouds [11, 56], particularly where appearance cues become critical for distinguishing geometrically similar objects.

Boundary-Aware Approaches. Starting from Gong *et al.* [13], recent boundary-aware frameworks such as JSENNet [19], CBL [47], and BFANet [63] explicitly learn boundary features to refine object boundaries in sparse point clouds [41]. These methods capture geometric discontinuities through dedicated boundary detection modules and edge-aware loss functions. However, they rely mainly on geometric cues and remain limited when segmentation requires appearance cues to address geometric bias arising from similar shapes but different materials.

Cross-Modal 2D-3D Fusion. To address the appearance deficiency, cross-modal 2D-3D fusion approaches leverage rich visual features from RGB images. Multi-view methods such as VMVF [27], 3DMV [8], and MVPNet [22] aggregate features from multiple viewpoints through pooling or attention mechanisms. Subsequent studies [5, 18, 20, 40] further explore bidirectional projection and pre-trained backbone fusion. However, these approaches are hindered by point-to-pixel alignment errors in occluded regions, projection-induced information loss, and spatial misalignment between sparse 3D distributions and dense 2D grids [15, 28]. Consequently, 2D-3D fusion struggles to fully unify appearance and geometry within native 3D space [12, 57].

2.2. Gaussian Splatting for 3D Segmentation

With the advent of 3D Gaussian Splatting (GS) [23], recent works leverage GS for 3D segmentation and scene understanding [3, 45, 58], and even for open-vocabulary or open-world perception [17, 21, 24, 31, 50, 54, 61]. Beyond improvements in rendering quality, efficiency, and compres-

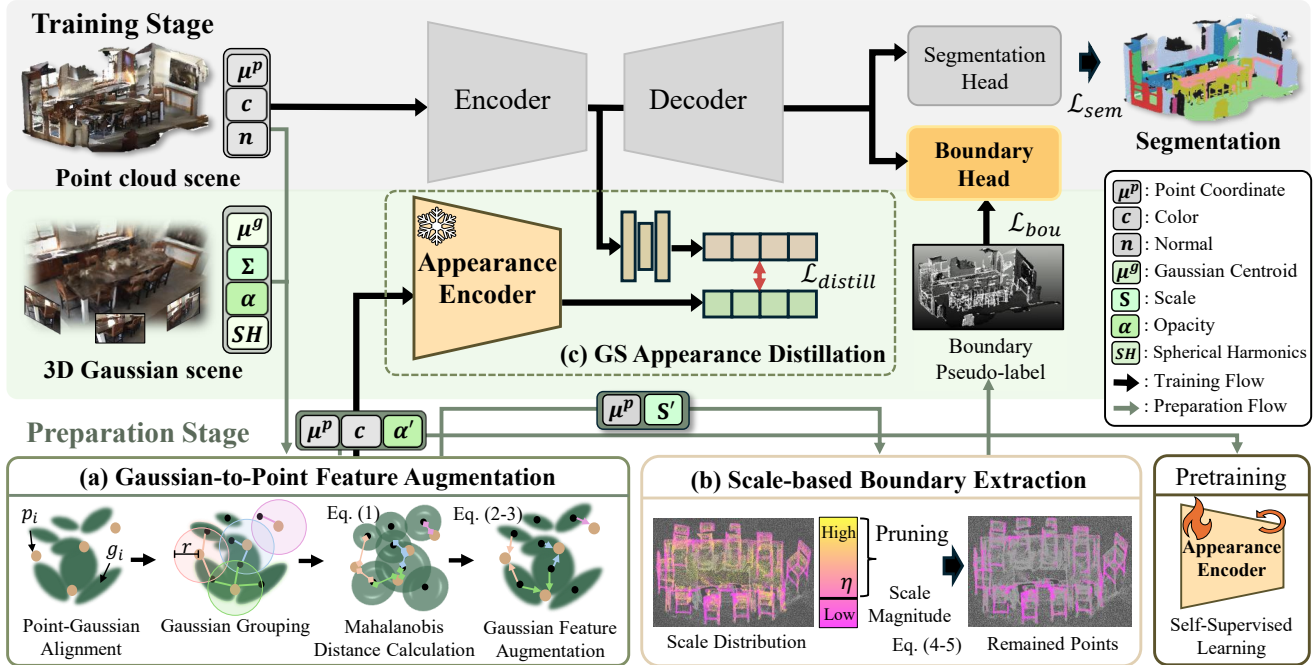


Figure 2. **Overview of the Gaussian-to-Point (G2P) learning approach.** G2P comprises a preparation stage and a main training stage. In the preparation stage, (a) Gaussian-to-Point Feature Augmentation aligns 3D Gaussian (μ^g, Σ, α) and point (μ^p, c, n), aggregating Gaussian attributes (α, S), where S represents the scale derived from the Σ , into augmented point features (α', S'). (b) Scale-based Boundary Extraction uses the aggregated Gaussian scale magnitude to derive boundary pseudo-labels. An appearance encoder is pre-trained in a self-supervised manner using the augmented point representation (μ^p, c, α'). In the training stage, (c) GS Appearance Distillation transfers appearance cues from the pre-trained encoder to the 3D segmentation model, which takes point cloud inputs (μ^p, c, n). The model is trained under joint supervision from semantic labels, boundary pseudo-labels, and appearance distillation.

sion, Gaussians encode continuous volumetric geometry and appearance in 3D scenes. By using this potential, numerous methods [38, 44, 65, 67] lift CLIP [39]-/SAM [25]-derived features or masks into GS and optimize segmentation within the Gaussian representation. These methods focus primarily on view-consistent rendering with segmented Gaussians, which serves a different objective from point cloud segmentation. They also provide no explicit Gaussian-to-point correspondences to preserve the original geometric structure, and instead serve as an intermediate representation for rendering purposes.

UniPre3D [49] targets point-level tasks, but relies on pixel-wise rendering losses combined with cross-modal fusion to pretrain a backbone network, treating Gaussians as an auxiliary self-supervised signal rather than producing supervised point-level outputs. By contrast, our G2P transfers GS attributes directly to points via explicit Gaussian-to-point alignment under 3D supervision, without requiring recourse to 2D priors or rendering-based losses. Prior evidence shows that these Gaussian attributes encode both appearance and geometric properties [30, 34, 62]. Building on this insight, G2P exploits them as complementary appearance and boundary cues, coupling the appearance richness

of Gaussians with the geometric stability of point clouds.

3. Method

3.1. Observation and Overview

In real-world 3D environments, numerous challenging classes lack clear geometric discriminability, which makes segmentation difficult. For example, doors and windows that are coplanar with walls, and appliances with reflective surfaces positioned adjacent to walls, are often geometrically indistinct from background structures. As shown in Fig. 1(a), the baseline model fails to distinguish between the refrigerator and the wall, misclassifying them as a single planar surface. Since these objects are primarily distinguishable by appearance cues such as color and texture, which are easily recognizable by human vision, learning representations solely based on geometry produces geometrically biased features.

To overcome the geometric bias of conventional methods, we propose Gaussian-to-Point (G2P), a unified learning approach that enriches point cloud representations with 3D Gaussian attributes. As illustrated in Fig. 2, G2P operates in two stages. In the Preparation Stage. (a) The

Gaussian-to-Point Feature Augmentation module (Sec. 3.3) aligns Gaussians with points and augments geometric and appearance attributes, while (b) the Scale-based Boundary Extraction (Sec. 3.4) derives boundary pseudo-labels from the aggregated scale distribution. With the augmented point clouds, we train an appearance encoder. In the Main Training Stage. (c) GS Appearance Distillation (Sec. 3.5) employs the pre-trained appearance encoder to transfer appearance features to the point cloud segmentation network. This design integrates complementary geometric and appearance information within a unified 3D representation while preserving the original point geometry.

3.2. Preliminaries

3D GS is a view synthesis method that models a 3D scene as a set of anisotropic Gaussians and renders images through alpha blending. Each Gaussian is parameterized by centroid μ^g , opacity α , spherical harmonics SH , and a covariance matrix Σ . The opacity α controls the blending contribution of each Gaussian along the ray, representing its visibility in the rendered view. The spatial shape of a Gaussian is defined by the covariance matrix $\Sigma = \mathbf{R}S\mathbf{R}^T$, where \mathbf{R} is a rotation matrix and \mathbf{S} is a diagonal scale matrix. The scale S determines the directional spread and geometric extent of the Gaussian in 3D space. We only use S as a geometric cue and α as appearance information from Gaussian primitives. For additional analysis of Gaussian attributes, please refer to the Supplementary. These choices ensure that G2P focuses on informative attributes that are available for all scenes.

3D GS produces a set of optimized 3D Gaussians whose coordinates are altered during adaptive density optimization. As a result, the original geometric structure of the input point cloud is lost, and point-level semantic labels become unusable [14, 23, 33, 43]. The resulting Gaussian scene exhibits substantially more noise and structural artifacts, such as indistinct edges, when compared to the cleaner input point cloud, making direct use for segmentation unreliable.

3.3. Gaussian-to-Point Feature Augmentation

To address these fundamental limitations, we propose the Gaussian-to-Point feature augmentation approach. This approach maintains the original point cloud geometry and instead aligns each point with its nearest 3D Gaussians. Each point is then augmented with the associated Gaussian attributes, enabling semantic segmentation while preserving geometric fidelity. To augment the point cloud $\mathcal{P} = \{p_i\}_{i=1}^N$, where each point $p_i = (\mu_i^p, c_i, n_i) \in \mathbb{R}^9$ consists of coordinates, color, and a normal vector, we transfer attributes from a set of 3D Gaussians $\mathcal{G} = \{g_j\}_{j=1}^M$. Both sets are first aligned in the same coordinate space. For each point p_i , we employ a two-stage process to iden-

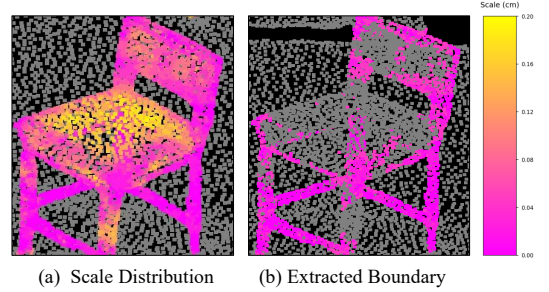


Figure 3. **Gaussian Scale distribution.** (a) Points after alignment, color-coded by aggregated Gaussian scale magnitude (magenta = small, yellow = large). Small scales concentrate at object boundaries. (b) Extracted boundary pseudo-labels by filtering out large-scale points.

tify its k most relevant Gaussian neighbors. First, to efficiently narrow down candidates, we select all Gaussians whose centroids fall within a Euclidean radius r of p_i . Second, within this candidate group, we compute the Mahalanobis distance [2] to each Gaussian. Unlike the Euclidean distance that assumes isotropic distributions, it incorporates each Gaussian’s anisotropic shape determined by its scale S and rotation R , providing a more physically plausible measure of proximity. The final k neighbors are selected based on the smallest Mahalanobis distances. Accordingly, the proposed weight parameter w_{ij} for each neighbor g_j is determined by the inverse of its Mahalanobis distance, normalized across the k neighbors:

$$w_{ij} = \frac{1/\sqrt{(\mu_i^p - \mu_j^g)^T \Sigma_j^{-1} (\mu_i^p - \mu_j^g)}}{\sum_{l=1}^k \left(1/\sqrt{(\mu_i^p - \mu_l^g)^T \Sigma_l^{-1} (\mu_i^p - \mu_l^g)} \right)}. \quad (1)$$

These weights are first used to aggregate the scale $S_j^g \in \mathbb{R}^3$ and opacity $\alpha_j^g \in \mathbb{R}$ attributes from the k neighbors. This yields the updated scale S_i^p and weighted opacity α_i^p for each point p_i :

$$S_i^p = \sum_{j=1}^k w_{ij} \cdot S_j^g, \quad \alpha_i^p = \sum_{j=1}^k w_{ij} \cdot \alpha_j^g. \quad (2)$$

This augmentation extends each point p_i to the form:

$$p_i = (\mu^p, c, n, S', \alpha') \in \mathbb{R}^{13}. \quad (3)$$

As a result, the point cloud \mathcal{P} is augmented with geometric S' and appearance α' attributes from the Gaussians. This attribute-augmented point cloud is further employed to facilitate appearance-guided representation learning and to derive scale-based boundary pseudo-labels.

3.4. Gaussian Scale-based Boundary Extraction

While geometric discontinuities can indicate boundaries, they fail for coplanar objects and thin structures that lack

clear geometric separation. We instead exploit Gaussian scale attributes, which encode surface extent: small scales naturally concentrate at object edges and boundaries, while large scales cover smooth planar regions (Fig. 3).

Following the attribute augmentation, we leverage the newly acquired scale features S'_i from the augmented point cloud \mathcal{P}' to extract boundary pseudo-labels. The scale of 3D Gaussians reflects object geometry, with large-scale Gaussians typically covering broad planar regions. Based on this, we identify boundaries by filtering out points with large aggregated scales. Specifically, we first create an object-focused point cloud, $\mathcal{P}'_{\text{obj}}$, by excluding points belonging to background classes (e.g., floor, wall) from \mathcal{P}' . For each point p'_i with its augmented scale vector $S'_i = (S'_x, S'_y, S'_z)$, we calculate its magnitude as the L2 norm:

$$\|S'_i\|_2 = \sqrt{S'_x^2 + S'_y^2 + S'_z^2}. \quad (4)$$

Using S'_i , we can now obtain the boundary pseudo-label subset $\mathcal{B}_{\text{scale}}$, which our scale-based approach identifies as the subset of $\mathcal{P}'_{\text{obj}}$ whose scale magnitude is below a dynamically determined threshold τ_η :

$$\mathcal{B}_{\text{scale}} = \{p'_i \in \mathcal{P}'_{\text{obj}} \mid \|S'_i\|_2 \leq \tau_\eta\}, \quad (5)$$

where the threshold τ_η is chosen to prune the top $\eta\%$ of points with the largest scale magnitudes, leaving the lower-scale points as boundary points.

To complement the geometric boundaries derived from scale, we also leverage semantic information. A point is identified as a semantic boundary candidate if any neighboring point within a local radius r has a different semantic label, forming the set \mathcal{B}_{sem} . To yield a more robust set of boundary labels for subsequent training, we merge geometric and semantic cues through a logical OR (union) operation, forming the final pseudo-labels as $\mathcal{B} = \mathcal{B}_{\text{scale}} \cup \mathcal{B}_{\text{sem}}$.

3.5. Gaussian Attribute-guided Learning

Appearance Encoder Pre-training. To preserve geometric consistency and prevent cross-modal misalignment, our approach takes point clouds as the sole input and receives appearance cues through feature distillation from a teacher encoder. To obtain such appearance representations, we re-purpose the Sonata [53] architecture to pre-train this teacher encoder **without pre-trained weights**. While Sonata is a self-supervised framework that independently trains an encoder, in our setup, we configure this framework to learn appearance features. Instead of using the traditional representation $p_i = (\mu_p, c, n)$ with 3D geometric normals $n \in \mathbb{R}^3$, we encode each point as $p_i = (\mu_p, c, \alpha)$, where $\alpha \in \mathbb{R}$ denotes opacity, introducing view-consistent appearance cues in place of geometric information. The encoder is trained from scratch on the corresponding dataset

Table 1. **Semantic segmentation on the ScanNet v2 validation set.** Methods are grouped by training approach. \dagger denotes results reproduced by us. $*$ indicates external pre-training beyond ScanNet v2. **Bold** denotes the best in each column.

Method	Venue	Method Type	mIoU \uparrow	mAcc \uparrow	OA \uparrow
VMVF* [27]	ECCV'20		76.4	–	–
BPNet [18]	CVPR'21		69.7	–	–
DeepViewAgg [40]	CVPR'22	2D-3D Fusion	71.0	–	–
PonderV2* [66]	TPAMI'25		77.0	–	–
UniPre3D \dagger * [49]	CVPR'25		77.6	85.0	92.1
ODIN (Swin-B)* [20]	CVPR'24		77.8	–	–
MinkUNet \dagger [7]	CVPR'19		72.3	80.2	90.0
OctFormer \dagger [48]	TOG'23		74.3	82.6	90.9
PT v3 \dagger [52]	CVPR'24	Geometric	77.0	84.3	92.1
BFANet \dagger [63]	CVPR'25		77.3	84.1	92.2
G2P (Ours)	–	GS-guided	78.4	85.2	92.5

(e.g., ScanNet v2 [9] or ScanNet++ [59]), ensuring dataset-specific pre-training for each benchmark. The pre-trained appearance encoder subsequently distills its representations into the 3D segmentation model that operates on point cloud $p_i = (\mu_p, c, n)$.

Our approach incorporates boundary information into semantic segmentation by adopting the boundary-semantic (B-S) block from BFANet [63] and integrating it into the PT v3 [52] backbone. The B-S block disentangles the intermediate features into semantic and boundary representations using independent MLPs and enhances semantic features by attending to boundary-aware queries.

Training Losses. Finally, the 3D segmentation model is trained using the proposed three supervisory signals: appearance, semantic, and boundary. For the appearance feature signal, we employ an additional mapping MLP ϕ , which takes the output features of the main point encoder, f_i^p , as input. We then distill knowledge from the features of the appearance encoder f_i^a by minimizing the cosine similarity loss, $\mathcal{L}_{\text{distill}}$ (the appearance distillation loss):

$$\mathcal{L}_{\text{distill}} = \frac{1}{N} \sum_{i=1}^N \left(1 - \frac{\phi(f_i^p) \cdot f_i^a}{\|\phi(f_i^p)\|_2 \|f_i^a\|_2} \right). \quad (6)$$

Semantic supervision loss, \mathcal{L}_{sem} , is applied via a combined loss of cross-entropy and Lovász-softmax [1], while boundary supervision loss, \mathcal{L}_{bou} , is provided using a combination of binary cross-entropy and Dice loss [35].

For these losses, we denote the ground truth semantic labels as y^g , boundary pseudo-labels as b^g , and the corresponding model predictions as \hat{p} and \hat{b} , respectively. Here, the loss functions are defined as:

$$\mathcal{L}_{\text{sem}} = \mathcal{L}_{\text{CE}}(y^g, \hat{p}) + \mathcal{L}_{\text{Lov}}(y^g, \hat{p}), \quad (7)$$

$$\mathcal{L}_{\text{bou}} = \mathcal{L}_{\text{BCE}}(b^g, \hat{b}) + \mathcal{L}_{\text{Dice}}(b^g, \hat{b}). \quad (8)$$

Table 2. **Class-wise IoU comparison on all ScanNet v2 categories.** **Red** and **blue** denote the best and second-best IoU, respectively. \dagger reproduced by us. **Avg.:** Average IoU for each subset. **Refrig.:** Refrigerator. **ShwrCurt.:** Shower Curtain.

Method	Geometrically Distinguishable Classes								Geometrically Challenging Classes							
	Wall	Floor	Cabinet	Bed	Chair	Sofa	Table	Bookshelf	Avg.	Door	Window	Picture	Curtain	Refrig.	ShwrCurt.	Avg.
MinkUNet \dagger [7]	87.1	96.7	67.0	83.4	92.6	84.5	77.0	81.4	83.7	70.4	65.0	37.8	77.2	64.0	67.2	63.6
OctFormer \dagger [48]	86.1	95.7	70.1	82.7	91.9	83.6	74.1	81.3	83.2	67.7	67.2	34.0	77.4	65.5	65.8	62.9
PT v3 \dagger [52]	87.7	95.8	73.0	83.2	93.1	83.7	78.9	80.6	84.5	74.6	72.8	41.8	77.9	64.9	68.9	66.8
UniPre3D [49]	87.5	95.5	72.6	84.4	92.7	84.9	80.0	82.3	85.0	74.6	72.6	38.5	79.0	70.3	76.3	68.6
BFANet \dagger [63]	87.2	95.7	72.3	84.7	92.5	83.0	81.2	80.6	84.7	74.0	73.5	38.5	77.5	69.3	70.8	67.3
G2P (Ours)	87.6	95.8	73.3	87.8	93.0	84.6	79.7	84.6	85.8	76.8	73.9	39.4	78.0	70.9	76.1	69.2

Table 3. **Semantic segmentation on the ScanNet200 validation set.** \dagger denotes reproduced results. $*$ indicates external pre-training beyond ScanNet v2. **Bold** denotes the best in each column.

Method	Venue	mIoU \uparrow	mAcc \uparrow	OA \uparrow
MinkUNet [7]	CVPR'19	25.0	32.9	80.4
PointContrast [55]	ECCV'20	26.2	—	—
OneFormer3D [26]	CVPR'24	30.1	—	—
PonderV2* [66]	TPAMI'25	32.3	—	—
OctFormer [48]	TOG'23	32.6	40.1	83.0
PT v3 \dagger [52]	CVPR'24	34.5	45.4	82.7
UniPre3D* [49]	CVPR'25	36.0	46.2	83.7
G2P (Ours)	—	36.6	46.0	83.8

The final loss, $\mathcal{L}_{\text{total}}$, is a weighted sum of the three terms, where λ_b and λ_d are weights balancing the boundary and distillation losses, respectively:

$$\mathcal{L}_{\text{total}} = \mathcal{L}_{\text{sem}} + \lambda_b \mathcal{L}_{\text{bou}} + \lambda_d \mathcal{L}_{\text{distill}}. \quad (9)$$

4. Experiments

4.1. Experiment Setting

Dataset. We evaluate our approach on the ScanNet v2 [9, 42], ScanNet++ [59], and Matterport3D [4] datasets. ScanNet v2, ScanNet200, ScanNet++, and Matterport3D contain 20, 200, 100, and 21 semantic classes, respectively. We report results on the validation splits of all datasets. For 3D Gaussian representations, we adopt the SceneSplat-7K [30] dataset, where each scene is reconstructed with approximately 1.5M Gaussian primitives. SceneSplat-7K provides GS reconstructions for indoor scenes, but outdoor environments are not available in the dataset.

Evaluation Metric. Following prior works [52, 63], we adopt three standard metrics for evaluation: mean Intersection over Union (mIoU), mean Accuracy (mAcc), and overall Accuracy (OA), measuring the percentage of correctly classified points across the entire dataset.

Implementation details. Our main training is conducted on a single NVIDIA RTX 3090 GPU for 800 epochs. The appearance encoder pre-training, following Sonata [53], is performed separately on an NVIDIA A6000 GPU for 400 epochs per dataset from scratch. We adopt Point Trans-

former v3 (PT v3) [52] as the backbone and incorporate the B-S block from BFANet [63]. The training batch size is set to 4, and we adopt Adam [32] as the optimizer with an initial learning rate of 0.003. All other settings follow PT v3, and detailed architectural configurations are reported in the Supplementary. For boundary pseudo-label extraction, we set the scale-based trimming ratio $\tau_\eta = 0.7$. The radius r for semantic boundary calculation is set to 4 cm. Loss weights are balanced as $\lambda_d = 0.4$, $\lambda_b = 0.9$.

4.2. Quantitative Comparison

Results on ScanNet v2. We compare G2P with geometric methods and 2D-3D fusion approaches on the ScanNet v2 validation set. Tab. 1 reports the results. G2P exceeds PT v3 by **+1.4** mIoU and BFANet [63] by **+1.1** under identical settings. G2P outperforms all geometric and 2D-3D fusion baselines without external pre-training. For reference, UniPre3D [49] and ODIN [20] both use external pre-training beyond ScanNet v2.

Class-wise analysis. To better understand where G2P excels, we categorize the 20 classes in ScanNet v2 into two groups based on geometric discriminability. *Geometrically challenging classes* include objects that are difficult to distinguish by geometry alone and are often coplanar with walls or exhibit reflective surfaces. *Geometrically distinguishable classes* include objects with clear structural features. As shown in Tab. 2, our G2P demonstrates superior performance on geometrically challenging classes with an average IoU of 69.2%. The largest class-level improvements occur on *refrigerator* (70.9 IoU, +6.0 vs. PT v3's 64.9) and *shower curtain* (+7.2).

Results on ScanNet200. We further evaluate on the ScanNet200 [42] validation set, which expands the label space from 20 to 200 fine-grained categories (Tab. 3). G2P attains **36.6** mIoU, **46.0** mAcc, and **83.8** OA, improving over our reproduced PT v3 [52] baseline by **+2.1** mIoU and remaining competitive with UniPre3D [49]. We do not report BFANet [63] on ScanNet200 due to the lack of official implementation for this dataset.

We further evaluate our method on the ScanNet200 hidden test set (Tab. 4). Following BFANet, we compare

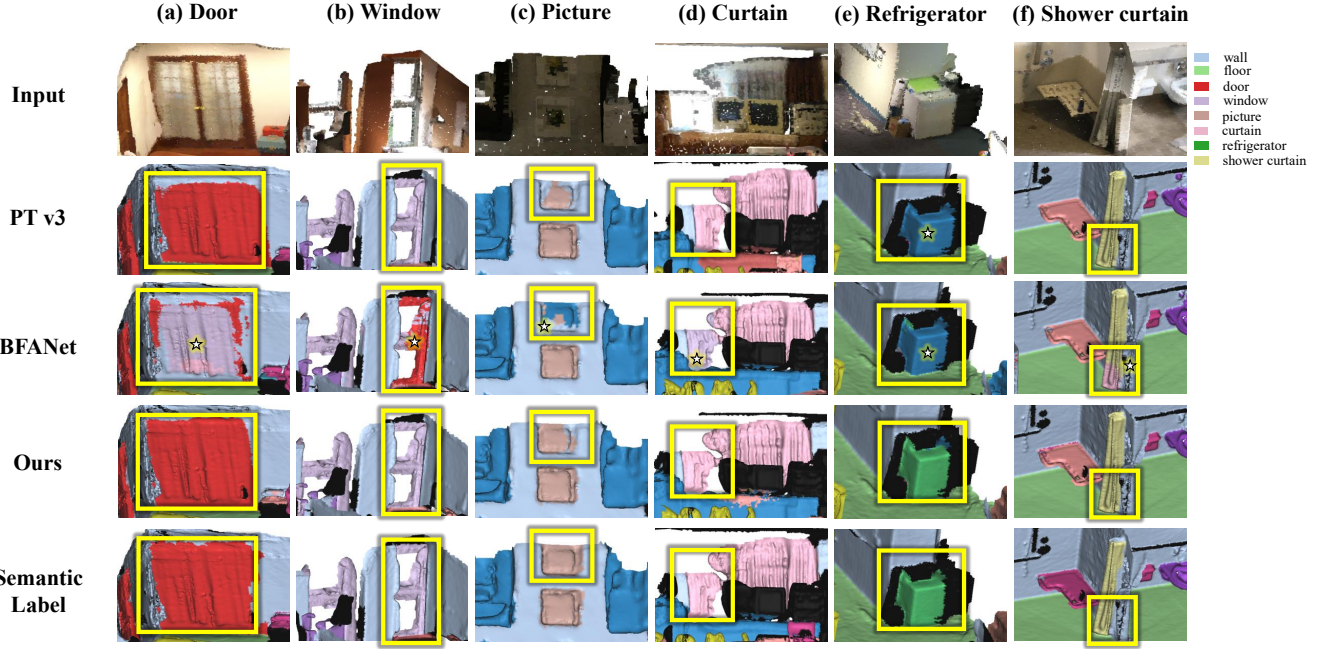


Figure 4. **Qualitative comparison on geometrically challenging classes in ScanNet v2.** **Yellow boxes** highlight regions with differing results between models. **Boxes with stars (\star)** indicate **category confusion**, where baselines misclassify objects (shown in **blue**) due to geometric bias (e.g., door \rightarrow wall, refrigerator \rightarrow cabinet). **Boxes without stars** indicate **incomplete segmentation**, where baselines fail to cover the full extent of thin or coplanar structures. G2P mitigates both failure modes through opacity-guided appearance distillation and scale-based boundary extraction. Corresponding regions in Ground Truth (bottom row) are marked for reference. Best viewed in color with zoom.

Table 4. **Evaluation on ScanNet200 Hidden Test Set.** We report mIoU, Head, Common, and Tail IoU on the official ScanNet200 benchmark (as of November 2025). **Red** and **blue** denote the best and second-best in each metric.

Method	Venue	mIoU	Head	Common	Tail
MinkUNet [7]	CVPR'19	25.3	46.3	15.4	10.6
OctFormer [48]	TOG'23	32.6	53.9	26.5	13.1
CeCo [64]	CVPR'23	34.0	55.1	24.7	18.1
PonderV2 [66]	CVPR'24	34.6	<u>55.2</u>	27.0	17.5
BFANet [63]	CVPR'25	36.0	55.3	29.3	19.3
G2P (Ours)	–	<u>35.5</u>	<u>55.3</u>	<u>28.6</u>	<u>18.7</u>

with methods that do not use large-scale pre-training beyond ScanNet v2. G2P achieves competitive performance with 35.5 mIoU, closely approaching BFANet’s 36.0 while matching it on Head classes and maintaining strong performance across Common and Tail categories.

4.3. Qualitative Comparisons

Qualitative results on challenging classes. Fig. 4 compares G2P with PT v3 [52] and BFANet [63] on challenging ScanNet v2 classes. Baselines exhibit two primary failure modes, highlighted by yellow boxes. **Boxes with stars (\star)** mark **category confusion**: in columns (a) *door* and (e) *refrigerator*, the baselines misclassify the objects as *wall* or *cabinet* due to coplanar geometry and similar textures. G2P correctly segments these objects. **Boxes without stars** mark **incomplete segmentation**: in columns (b) *window*, (c) *picture*, (d) *curtain*, and (f) *shower curtain*, baselines fail to cover the full extent of thin structures. G2P produces sharper, more complete masks for these objects. These trends align with Tab. 2, where G2P achieves substantial gains on *refrigerator* (improvements of 6.0% in IoU vs. PT v3), confirming that G2P effectively mitigates both failure modes.

Table 5. **Module ablation on ScanNet v2.** (a) Baseline uses pure geometric features. (b) adds *boundary guidance* to improve localization on coplanar and thin structures. (c) adds *appearance distillation* to stabilize semantic consistency in category interiors.

Method	Components		Performance	
	Boundary Guidance	Appearance Distillation	mIoU \uparrow	OA \uparrow
(a)			77.0	92.1
(b)	✓		77.8	92.1
(c)		✓	77.8	92.0
G2P (Ours)	✓	✓	78.4	92.5

refrigerator, the baselines misclassify the objects as *wall* or *cabinet* due to coplanar geometry and similar textures. G2P correctly segments these objects. **Boxes without stars** mark **incomplete segmentation**: in columns (b) *window*, (c) *picture*, (d) *curtain*, and (f) *shower curtain*, baselines fail to cover the full extent of thin structures. G2P produces sharper, more complete masks for these objects. These trends align with Tab. 2, where G2P achieves substantial gains on *refrigerator* (improvements of 6.0% in IoU vs. PT v3), confirming that G2P effectively mitigates both failure modes.

Table 6. **Results on ScanNet++ and Matterport3D.** All models are trained and evaluated within each dataset. **Bold** indicates the best in each column. \dagger denotes reproduced results.

Method	ScanNet++ (val)			Matterport3D (val)		
	mIoU \uparrow	mAcc \uparrow	OA \uparrow	mIoU \uparrow	mAcc \uparrow	OA \uparrow
PT v3 \dagger [52]	47.9	59.1	90.0	55.5	64.9	82.1
G2P (Ours)	48.7	60.1	90.0	55.9	66.4	82.2

Table 7. **Ablation on strategies for Gaussian primitive (opacity)**

Learning. We compare: (i) *Raw 3D Gaussians*, which use Gaussian primitives as direct training inputs; (ii) *Points with Opacity*, which also provide point features and their Gaussian opacity directly to the model; and (iii) *G2P (Ours)*, which distills Gaussian appearance to the segmentation model. All models are evaluated on ScanNet v2 validation set.

Method	Learning	Input Attributes	mIoU \uparrow
Raw 3D Gaussians	Direct input	x^g, c', n', α	73.1
Points with Opacity	Direct input	x^p, c, n, α'	77.3
G2P (Ours)	Distillation	x^p, c, n, α'	77.8

4.4. Ablation Studies

Module ablation. We conduct ablation studies to validate the contribution of each component (Tab. 5). Both boundary guidance and appearance distillation independently improve mIoU, with their combination achieving the highest gain. This confirms that boundary and appearance cues from 3D Gaussians provide complementary benefits. Each component alone produces competitive results, and combining them yields the most reliable segmentation by reducing boundary leakage and false merges.

Results on Additional Benchmarks. To further validate G2P’s effectiveness, we evaluate on the ScanNet++ [59] and Matterport3D [4] validation sets. As shown in Tab. 6, G2P generalizes well across datasets, achieving 48.7 and 55.9 mIoU on ScanNet++ and Matterport3D, outperforming PT v3 by +0.8 and +0.4.

Appearance transfer. Tab. 7 evaluates strategies for leveraging Gaussian appearance features. Using raw Gaussian coordinates proves unreliable for point-level segmentation (73.1 mIoU). In contrast, *Points with Opacity* improves performance to 77.3 mIoU, demonstrating that Gaussian appearance carries useful cues for segmentation. Our distilled variant reaches the highest mIoU of 77.8 and removes the need for Gaussian features at inference, in contrast to *Points with Opacity* method.

Correspondence metric. Gaussian-to-point correspondence depends on the distance metric and the neighborhood size k . Euclidean distance ignores the anisotropy of splats and yields unstable matches near object bound-

Table 8. **Ablation on distance metric and neighborhood size for Gaussian-to-point feature augmentation (ScanNet v2).** This experiment examines how different correspondence settings, including distance metric and the neighborhood size k , influence the alignment of Gaussian primitives to points during feature augmentation, which subsequently affects appearance encoder pre-training and boundary extraction.

Method	mIoU \uparrow	mAcc \uparrow	OA \uparrow
Euclidean Distance	77.0	84.4	91.8
Mahalanobis ($k = 10$)	77.4	85.3	92.0
Mahalanobis ($k = 20$)	78.4	85.2	92.5
Mahalanobis ($k = 30$)	77.9	85.3	92.1

Table 9. **Model efficiency on ScanNet v2.** Comparison of training and inference efficiency between PT v3 and G2P. \dagger denotes reproduced results.

Method	Params.	Training		Inference		mIoU \uparrow
		Latency	Memory	Latency	Memory	
MinkUNet \dagger [7]	39.2M	71ms	1.6G	29ms	1.4G	72.3
OctFormer \dagger [48]	44.0M	259ms	4.2G	94ms	4.4G	74.3
PT v3 \dagger [52]	46.2M	132ms	5.6G	79ms	1.9G	77.0
G2P (Ours)	46.4M	220ms	7.3G	96ms	3.3G	78.4

aries. Mahalanobis distance leverages the covariance Σ to form tighter, more reliable matches. As shown in Tab. 8, a moderate neighborhood ($k = 20$) offers the best trade-off (78.4 mIoU, 92.5 OA). Smaller k is noisy, whereas larger k oversmooths labels. These results support covariance-aware matching as the default in G2P.

Inference efficiency. Tab. 9 evaluates computational efficiency. Training G2P incurs additional overhead due to appearance distillation: training latency increases from 132ms to 220ms (+67%) and memory usage from 5.6GB to 7.3GB (+30%). However, inference overhead remains moderate: parameters increase by only 0.2M (+0.4%), latency increases from 79ms to 96ms (+21%), and memory usage increases from 1.9GB to 3.3GB (+74%).

5. Conclusion

We presented G2P, a novel approach for point cloud semantic segmentation that integrates 3D Gaussian Splatting to unify geometric and appearance cues in 3D space. Our three-component approach, comprising Gaussian-to-point feature augmentation, opacity-guided appearance learning, and scale-based boundary extraction, addresses the fundamental geometric bias. By augmenting point features with Gaussian attributes, G2P enhances semantic segmentation on point clouds, particularly for objects that are geometrically ambiguous but have distinctive appearances. Extensive experiments on standard benchmarks demonstrate state-of-the-art performance and strong generaliza-

tion across datasets. Furthermore, we conduct ablations to validate the effectiveness of GS-guided feature augmentation, establishing its practical value for 3D scene understanding.

References

- [1] Maxim Berman, Amal Rannen Triki, and Matthew B. Blaschko. The lovasz-softmax loss: A tractable surrogate for the optimization of the intersection-over-union measure in neural networks. In *CVPR*, pages 4413–4421, 2018. [5](#)
- [2] Anil Bhattacharyya. On a measure of divergence between two multinomial populations. *Sankhyā: The Indian Journal of Statistics*, pages 401–406, 1946. [4](#)
- [3] Jing Cen, Jiayu Fang, Chen Yang, Lingxi Xie, Xingang Zhang, Wei Shen, and Qi Tian. Segment any 3d gaussians. In *AAAI*, pages 1971–1979, 2025. [2](#)
- [4] Angel X. Chang, Angela Dai, Thomas Funkhouser, Maciej Halber, Matthias Nießner, Manolis Savva, Yinda Zhang, et al. Matterport3d: Learning from rgb-d data in indoor environments. *arXiv preprint arXiv:1709.06158*, 2017. [6, 8](#)
- [5] Zhen Chen, Liang Jing, Yixin Li, and Bing Li. Bridging the domain gap: Self-supervised 3d scene understanding with foundation models. In *NeurIPS*, pages 79226–79239, 2023. [2](#)
- [6] Hao-Yu Chiang, Yu-Lun Lin, Yen-Cheng Liu, and Winston H. Hsu. A unified point-based framework for 3d segmentation. In *3DV*, pages 155–163. IEEE, 2019. [1](#)
- [7] Christopher Choy, JunYoung Gwak, and Silvio Savarese. 4d spatio-temporal convnets: Minkowski convolutional neural networks. In *CVPR*, pages 3075–3084, 2019. [1, 2, 5, 6, 7, 8](#)
- [8] Angela Dai and Matthias Nießner. 3dmv: Joint 3d-multi-view prediction for 3d semantic scene segmentation. In *ECCV*, pages 452–468. Springer, 2018. [2](#)
- [9] Angela Dai, Angel X. Chang, Manolis Savva, Maciej Halber, Thomas Funkhouser, and Matthias Nießner. Scannet: Richly-annotated 3d reconstructions of indoor scenes. In *CVPR*, pages 5828–5839, 2017. [5, 6](#)
- [10] Angela Dai, Matthias Nießner, Michael Zollhöfer, Shahram Izadi, and Christian Theobalt. Bundlefusion: Real-time globally consistent 3d reconstruction using on-the-fly surface reintegration. *ACM TOG*, 36(4):1, 2017. [1](#)
- [11] Zhiheng Fang, Cheng Zhuang, Zhiyuan Lu, Yifan Wang, Liang Liu, and Jing Xiao. Bgpseg: Boundary-guided primitive instance segmentation of point clouds. *IEEE TIP*, 2025. [2](#)
- [12] Kyle Genova, Xi Yin, Abhijit Kundu, Caroline Pantofaru, Forrester Cole, Avneesh Sud, and Thomas Funkhouser. Learning 3d semantic segmentation with only 2d image supervision. In *3DV*, pages 361–372. IEEE, 2021. [2](#)
- [13] Jiaqi Gong, Jun Xu, Xin Tan, Jiahua Zhou, Yifan Qu, Yu Xie, and Linjsenet Ma. Boundary-aware geometric encoding for semantic segmentation of point clouds. In *AAAI*, pages 1424–1432, 2021. [2](#)
- [14] Antoine Guédon and Vincent Lepetit. Sugar: Surface-aligned gaussian splatting for efficient 3d mesh reconstruction and high-quality mesh rendering. In *CVPR*, pages 5354–5363, 2024. [2, 4](#)
- [15] Yulan Guo, Huan Wang, Qingyong Hu, Hao Liu, Li Liu, and Mohammed Bennamoun. Deep learning for 3d point clouds: A survey. *IEEE TPAMI*, 43(12):4338–4364, 2020. [1, 2](#)
- [16] Zhaoxi Han, Mohamed El Amine Boudjoghra, Jun Dong, Jiahao Wang, and Rao Muhammad Anwer. All in one: Visual-description-guided unified point cloud segmentation. In *ICCV*, pages 24835–24845, 2025. [1](#)
- [17] Shilong He, Gu Jie, Cheng Wang, Yuxiang Zhou, Shuai Hu, Guoliang Li, and Haibin Ding. Refersplat: Referring segmentation in 3d gaussian splatting. *arXiv preprint arXiv:2508.08252*, 2025. [2](#)
- [18] Wei Hu, Hang Zhao, Li Jiang, Jiaya Jia, and Tien-Tsin Wong. Bidirectional projection network for cross dimension scene understanding. In *CVPR*, pages 14373–14382, 2021. [2, 5](#)
- [19] Ziyang Hu, Mengyuan Zhen, Xiang Bai, Hongbo Fu, and Chiew-Lan Tai. Jsenet: Joint semantic segmentation and edge detection network for 3d point clouds. In *ECCV*, pages 222–239. Springer, 2020. [1, 2](#)
- [20] Ayush Jain, Prannay Katara, Nikolaos Gkanatsios, Adam W. Harley, Gabriele Sarch, Kriti Aggarwal, and Katerina Fragkiadaki. Odin: A single model for 2d and 3d segmentation. In *CVPR*, pages 3564–3574, 2024. [1, 2, 5, 6](#)
- [21] Seunghyun Jang and Wooyoung Kim. Identity-aware language gaussian splatting for open-vocabulary 3d semantic segmentation. In *ICCV*, pages 20467–20476, 2025. [2](#)
- [22] Maxime Jaritz, Jiayuan Gu, and Hao Su. Multi-view pointnet for 3d scene understanding. In *ICCVW*, 2019. [1, 2](#)
- [23] Bernhard Kerbl, Georgios Kopanas, Thomas Leimkühler, and George Drettakis. 3d gaussian splatting for real-time radiance field rendering. *ACM TOG*, 42(4):1–14, 2023. [2, 4](#)
- [24] Jun-Seong Kim, Gwangsu Kim, Yu-Ji Kim, Yu-Chiang Frank Wang, Jaehoon Choe, and Tae-Hyun Oh. Dr. splat: Directly referring 3d gaussian splatting via direct language embedding registration. In *CVPR*, pages 14137–14146, 2025. [2](#)
- [25] Alexander Kirillov, Eric Mintun, Nikhila Ravi, Hanzi Mao, Chloe Rolland, Laurens Gustafson, Tete Xiao, Sam Whitehead, Alexander C. Berg, Wan-Yen Lo, Piotr Dollár, and Ross Girshick. Segment anything. In *ICCV*, pages 4015–4026, 2023. [3](#)
- [26] Maksym Kolodiaznyi, Alena Vorontsova, Anton Konushin, and Daniil Rukhovich. Oneformer3d: One transformer for unified point cloud segmentation. In *CVPR*, pages 20943–20953, 2024. [1, 6](#)
- [27] Abhijit Kundu, Xiaoyang Yin, Alireza Fathi, David Ross, Bradley Brewington, Thomas Funkhouser, and Caroline Pantofaru. Virtual multi-view fusion for 3d semantic segmentation. In *ECCV*, pages 518–535. Springer, 2020. [2, 5](#)
- [28] H. Kweon and Kuk-Jin Yoon. Joint learning of 2d-3d weakly supervised semantic segmentation. In *NeurIPS*, pages 30499–30511, 2022. [2](#)
- [29] Yangyan Li, Rui Bu, Mingchao Sun, Wei Wu, Xin Di, and Baoquan Chen. Pointcnn: Convolution on x-transformed points. In *NeurIPS*, 2018. [2](#)
- [30] Yuxuan Li, Qianyu Ma, Ruichi Yang, Haoxuan Li, Ming Ma, Boxun Ren, and Deepak P. Paudel. Scenesplat: Gaussian splatting-based scene understanding with vision-language

pretraining. *arXiv preprint arXiv:2503.18052*, 2025. 2, 3, 6

[31] Zhenyu Liu, Yan Wang, Shuchang Zheng, Tianyi Pan, Lihua Liang, Yanwei Fu, and Xiangyang Xue. Reasongrounder: LvLM-guided hierarchical feature splatting for open-vocabulary 3d visual grounding and reasoning. In *CVPR*, pages 3718–3727, 2025. 2

[32] Ilya Loshchilov and Frank Hutter. Decoupled weight decay regularization. *arXiv preprint arXiv:1711.05101*, 2017. 6

[33] Tianwei Lu, Ming Yu, Linghao Xu, Yuanhan Xiangli, Lijie Wang, Dahua Lin, and Bo Dai. Scaffold-gs: Structured 3d gaussians for view-adaptive rendering. In *CVPR*, pages 20654–20664, 2024. 2, 4

[34] Qian Ma, Yujing Li, Bo Ren, Nicu Sebe, Ender Konukoglu, Theo Gevers, and Dharma P. Paudel. Shapesplat: A large-scale dataset of gaussian splats and their self-supervised pre-training. *arXiv preprint arXiv:2408.10906*, 2024. 3

[35] Fausto Milletari, Nassir Navab, and Seyed-Ahmad Ahmadi. V-net: Fully convolutional neural networks for volumetric medical image segmentation. In *2016 fourth international conference on 3D vision*, pages 565–571. Ieee, 2016. 5

[36] Charles R. Qi, Hao Su, Kaichun Mo, and Leonidas J. Guibas. Pointnet: Deep learning on point sets for 3d classification and segmentation. In *CVPR*, pages 652–660, 2017. 2

[37] Charles R. Qi, Li Yi, Hao Su, and Leonidas J. Guibas. Pointnet++: Deep hierarchical feature learning on point sets in a metric space. In *NeurIPS*, 2017. 2

[38] Mingyuan Qin, Wenqiang Li, Jingwei Zhou, Huan Wang, and Hanspeter Pfister. Langsplat: 3d language gaussian splatting. In *CVPR*, pages 20051–20060, 2024. 3

[39] Alec Radford, Jong Wook Kim, Chris Hallacy, Aditya Ramesh, Gabriel Goh, Sandhini Agarwal, Girish Sastry, Amanda Askell, Pamela Mishkin, Jack Clark, Gretchen Krueger, and Ilya Sutskever. Learning transferable visual models from natural language supervision. In *ICML*, pages 8748–8763, 2021. 3

[40] Dorian Robert, Bruno Vallet, and Loic Landrieu. Learning multi-view aggregation in the wild for large-scale 3d semantic segmentation. In *CVPR*, pages 5575–5584, 2022. 1, 2, 5

[41] Wooseok Roh, Hyunho Jung, Gyuwon Nam, Jinyeong Yeom, Hyunsung Park, Seunghyun Yoon, and Sunghoon Kim. Edge-aware 3d instance segmentation network with intelligent semantic prior. In *CVPR*, pages 20644–20653, 2024. 2

[42] David Rozenberszki, Or Litany, and Angela Dai. Language-grounded indoor 3d semantic segmentation in the wild. In *ECCV*, pages 125–141. Springer, 2022. 6

[43] Cheng Ruan, Yifan Wang, Tao Guan, Bin Zhang, and Lili Ju. Indoorgs: Geometric cues guided gaussian splatting for indoor scene reconstruction. In *CVPR*, pages 844–853, 2025. 2, 4

[44] Hongyi Shen, Jing Ni, Yifan Chen, Weijia Li, Ming Pei, and Shuang Huang. Trace3d: Consistent segmentation lifting via gaussian instance tracing. In *ICCV*, pages 6656–6666, 2025. 3

[45] Qian Shen, Xia Yang, and Xin Wang. Flashsplat: 2d to 3d gaussian splatting segmentation solved optimally. In *ECCV*, pages 456–472, Cham, 2024. ECCV. 2

[46] Hang Su, Subhransu Maji, Evangelos Kalogerakis, and Erik Learned-Miller. Multi-view convolutional neural networks for 3d shape recognition. In *ICCV*, pages 945–953, 2015. 1

[47] Liang Tang, Yizhou Zhan, Zilong Chen, Baosheng Yu, and Dacheng Tao. Contrastive boundary learning for point cloud segmentation. In *CVPR*, pages 8489–8499, 2022. 1, 2

[48] Peng-Shuai Wang. Octformer: Octree-based transformers for 3d point clouds. *ACM TOG*, 42(4):1–11, 2023. 1, 2, 5, 6, 7, 8

[49] Zeyu Wang, Yifan Zhang, Jingbo Zhou, and Jiwen Lu. Uniprep3d: Unified pre-training of 3d point cloud models with cross-modal gaussian splatting. In *CVPR*, pages 1319–1329, 2025. 3, 5, 6

[50] Lukas Wiedmann, Lennart Wiehe, and Dániel Rozenberszki. Dcseg: Decoupled 3d open-set segmentation using gaussian splatting. In *CVPR*, pages 5217–5226, 2025. 2

[51] Wenzuan Wu, Zhongang Qi, and Li Fuxin Li. Pointconv: Deep convolutional networks on 3d point clouds. In *CVPR*, pages 9621–9630, 2019. 2

[52] Xiaoqi Wu, Li Jiang, Peng-Shuai Wang, Zhirong Liu, Xiao Liu, Yu Qiao, and Hang Zhao. Point transformer v3: Simpler faster stronger. In *CVPR*, pages 4840–4851, 2024. 1, 2, 5, 6, 7, 8

[53] Xiaoyu Wu, Daniel DeTone, Daniel Frost, Tianwei Shen, Chenshen Xie, Nan Yang, and Julian Straub. Sonata: Self-supervised learning of reliable point representations. In *CVPR*, pages 22193–22204, 2025. 2, 5, 6

[54] Yifan Wu, Jie Meng, Hongwei Li, Chao Wu, Yujie Shi, Xiaowei Cheng, and Jiahui Zhang. Opengaussian: Towards point-level 3d gaussian-based open vocabulary understanding. In *NeurIPS*, pages 19114–19138, 2024. 2

[55] Sangwoo Xie, Jiayuan Gu, Dongze Guo, Charles R. Qi, Leonidas Guibas, and Or Litany. Pointcontrast: Unsupervised pre-training for 3d point cloud understanding. In *ECCV*, pages 574–591. Springer, 2020. 2, 6

[56] Mingye Xu, Zhipeng Zhou, Junhao Zhang, and Yu Qiao. Investigate indistinguishable points in semantic segmentation of 3d point cloud. In *Proceedings of the AAAI Conference on Artificial Intelligence*, pages 1612–1620, 2021. 2

[57] Cheng-Kuang Yang, Ming-Hsuan Chen, Yung-Yu Chuang, and Yu-Chiang Frank Lin. 2d-3d interlaced transformer for point cloud segmentation with scene-level supervision. In *ICCV*, pages 977–987, 2023. 2

[58] Mao Ye, Martin Danelljan, Fisher Yu, and Lei Ke. Gaussian grouping: Segment and edit anything in 3d scenes. In *ECCV*, pages 162–179. Springer, 2024. 2

[59] Chethan Yeshwanth, Yunchao Liu, Matthias Nießner, and Angela Dai. Scannet++: A high-fidelity dataset of 3d indoor scenes. In *ICCV*, pages 12–22, 2023. 5, 6, 8

[60] Zehao Yu, Torsten Sattler, and Andreas Geiger. Gaussian opacity fields: Efficient adaptive surface reconstruction in unbounded scenes. In *ECCV*, 2024. 2

[61] Haoran Zhai, Haoyu Li, Zheng Li, Xin Pan, Yifan He, and Guangyao Zhang. Panogs: Gaussian-based panoptic seg-

mentation for 3d open vocabulary scene understanding. In *CVPR*, pages 14114–14124, 2025. 2

[62] Ruofan Zhang, Hengrui Zhu, Ji Zhao, Qi Zhang, Xiaoguang Cao, and Zhigang Ma. Mitigating ambiguities in 3d classification with gaussian splatting. In *CVPR*, pages 27275–27284, 2025. 2, 3

[63] Wen Zhao, Rui Zhang, Qixiang Wang, Gong Cheng, and Ke Huang. Bfanet: Revisiting 3d semantic segmentation with boundary feature analysis. In *CVPR*, pages 29395–29405, 2025. 1, 2, 5, 6, 7

[64] Zhisheng Zhong, Jiequan Cui, Yibo Yang, Xiaoyang Wu, Xiaojuan Qi, Xiaogang Zhang, and Jiaya Jia. Understanding imbalanced semantic segmentation through neural collapse. In *CVPR*, pages 19550–19560, 2023. 7

[65] Shuo Zhou, Hongje Chang, Shuaifeng Jiang, Zhiwen Fan, Zhengqin Zhu, Danfei Xu, and Achuta Kadambi. Feature 3dgs: Supercharging 3d gaussian splatting to enable distilled feature fields. In *CVPR*, pages 21676–21685, 2024. 3

[66] Haoyi Zhu, Honghui Yang, Xiaoyang Wu, Di Huang, Sha Zhang, Xianglong He, and Wanli Ouyang. Ponderv2: Pave the way for 3d foundation model with a universal pre-training paradigm. *arXiv preprint arXiv:2310.08586*, 2023. 5, 6, 7

[67] Rui Zhu, Shuchen Qiu, Ziwei Liu, Ka Hin Hui, Qi Wu, Pheng Ann Heng, and Chi-Wing Fu. Rethinking end-to-end 2d to 3d scene segmentation in gaussian splatting. In *CVPR*, pages 3656–3665, 2025. 3